Crazing in Two and Three Dimensions. 2. Three-Dimensional Crazing

T. N. Krupenkin*

Bell Labs, Lucent Technologies, 600 Mountain Avenue, Murray Hill, New Jersey 07974

G. H. Fredrickson

Materials Research Laboratory, University of California, Santa Barbara, California 93106

Received June 29, 1998; Revised Manuscript Received April 1, 1999

ABSTRACT: Crazing in thick polymer glass films and bulk glassy polymers is theoretically investigated. A simple microscopic model that treats an amorphous polymer at stresses above the yield stress as a viscous fluid with the scale-dependent surface tension is developed. Craze microstructural parameters including fibril diameter, spacing, and draw ratio are calculated. Crazing stress and critical thickness are determined as functions of material parameters and conditions of testing. The obtained results are in good quantitative agreement with experimental data.

1. Introduction

In the first part of the present series, we were concerned with the theoretical description of craze thickening in very thin polymer films. In particular, we discussed the so-called two-dimensional (2D) crazes encountered in polymer glass films with thicknesses below a certain critical thickness.[14,15] We now want to establish a connection between such 2D crazes and regular (or 3D) crazes that are found in thick films and bulk polymers. Although our main goal remains the same as in part one, i.e., to provide a theoretical description of the critical thickness and related phenomena, we will also try to improve on the existing results due to Kramer et al. concerning prediction of the 3D craze microstructure and craze-thickening stress.[24,25] In particular, we would like to obtain a better understanding of the dependence of the craze-thickening stress and the craze fibril diameter on the polymer entanglement density and temperature. Another point of interest is quantitative description of the craze-to-shear transition at different entanglement densities and temperatures. Similar to what was done in Part 1, we reduce the problem to the case where no chain pullout is possible; i.e., we restrict ourselves to the case of temperatures well below the glass-transition temperature T_g and polymer molecular weights well above the entanglement molecular weight.

A typical structure of a regular 3D craze in a glassy polymer is schematically shown in Figure 1 of Part 1. It consists of a network of thin fibrils with typical diameters on the order of 10−20 nm that are occasionally connected by short cross-ties.[24−27] There is a variety of experimental data on craze thickening phenomenon available in the literature.[2−33] The craze-thickening stress σ_0 is known to be a function of several variables including strain rate $\dot{\epsilon}$, temperature T, and polymer density of entanglements ν. Experiments[26,27] show that crazing stress σ_0 decreases linearly with T, at least when T is not too close to the glass-transition temperature T_g. Craze-thickening stress σ_0 increases with entanglement density ν, at least for low and moderate $\nu \lesssim 10 \times 10^{25}$−$12 \times 10^{25}$ m^{-3}; see Figure 1. The natural draw ratio of craze fibrils λ_m correlates well with the maximum microscopically allowed extension λ_{st} of the average entanglement strand[24] and is approximately equal to $0.9\lambda_{st}$. The value of λ_m does not depend on temperature,[24] unless T approaches T_g. Mean fibril spacing and fibril diameter are also independent of temperature[24] for T not too close to T_g. If the craze propagation stress σ_0 exceeds the shear (yield) stress σ_y, a craze-to-shear transition occurs. This happens as one increases either T or ν; see Figure 2. Furthermore, if one decreases the sample thickness below some critical value, a transition from 3- to 2D crazing occurs. This is usually referred to as the phenomenon of critical thickness.[1,34−37] A plot of the critical sample thickness D_c below which no 3D crazing can occur is shown in Figure 3 for various polymers as a function of their entanglement density.

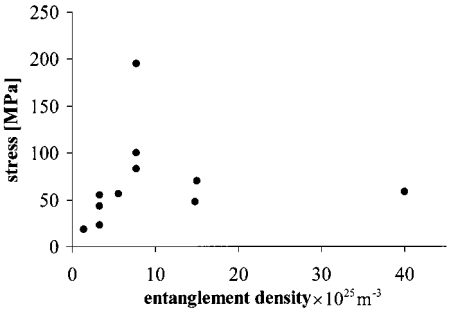

Figure 1. Crazing stress σ_0 for various polymers plotted as a function of their entanglement density ν. Data from refs 24−31.

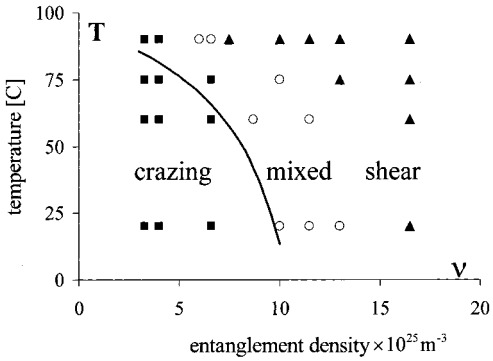

Figure 2. Modes of deformation in pure and cross-linked PS. Squares correspond to pure crazes, circles to mixed deformation mode, and triangles to pure shear. Data from ref 24. Solid curve corresponds to eq 50; see details in section 8.

10.1021/ma9810159 CCC: $18.00 © 1999 American Chemical Society
Published on Web 07/09/1999

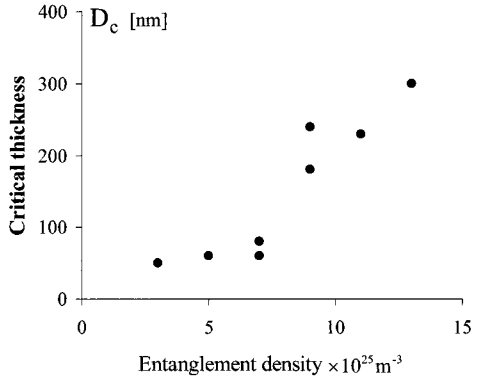

Figure 3. Critical thickness for various PS/PPO blends plotted as a function of their entanglement density. Data from refs 34−37.

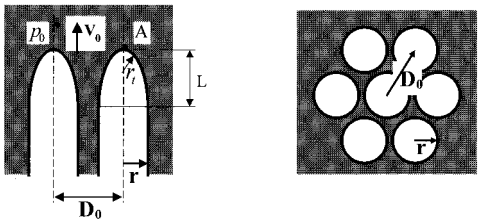

Figure 4. 3D craze described as a set of void fingers propagating through the polymer. The top of the finger has an ellipsoidal shape with semi-axes L and r. The radius of the curvature at the top is r_t. The void fingers are arranged on a hexagonal lattice with the finger separation equal to D_0.

Our first goal is to construct the model describing microstructural parameters of a 3D craze, such as fibril diameter D_0 and draw ratio λ_m, as well as the dependence of crazing stress σ_0 on entanglement density ν and temperature T. As a second step, the results obtained are used to describe the phenomenon of critical thickness and the craze-to-shear transition. The paper is organized in the following manner. In the next section, we discuss the model that is used to describe 3D crazes. A definition of the surface tension as applied to this model is given in section 3. Two important limiting cases of noninteracting and strongly interacting fingers are discussed in sections 4 and 5. The parameters of the fastest propagating finger are investigated in section 6. Craze microstructure and crazing stress are discussed in sections 7 and 8. The phenomenon of critical thickness is addressed in section 9. Finally, conclusions are given in section 10.

2. Model

Similar to the theorists of earlier craze models,[24,25] we describe a regular 3D craze structure as a set of void fingers propagating through the material with a constant velocity v_0 under the influence of the craze thickening stress σ_0, as shown in Figure 4. We assume that the thin walls separating neighboring fingers lose their stability at some distance from the finger top and develop holes that connect neighboring fingers. When the holes are big enough, the resulting system of interconnected void fingers becomes similar to the structure commonly used to describe crazes, i.e., to the set of parallel fibrils connected by short cross-ties. As we will see later, the material within these fibrils is highly elongated and thus does not allow any further fibril thinning as the craze continues to widen. In the present model, we are primarily concerned with the description of a steady-state propagation of the fingers and do not address various processes that define the fine fibril structure, such as the process of creation of holes just outlined above. We also consider only craze-thickening stress σ_0, that is, the stress at the immediate vicinity of the craze boundary, and do not address the problem of the relationship between σ_0 and the general stress state of the sample.

We describe an individual finger as a cylinder with the ellipsoidal cap at the top. For simplicity, we assume that the fingers are arranged on a hexagonal lattice as shown in Figure 4, but the model can be reformulated for any arrangement, including a random one. Similar to the model of 2D crazing described in Part 1, the present model describes a polymer glass at stresses above the yield stress as a Newtonian fluid with some effective viscosity η, which corresponds to the chosen characteristic strain rate. Thus, we reduce our problem to the problem of the void finger propagation in a viscous fluid. For this problem, it was shown[40] that the surface tension and hydrodynamic forces dominate finger propagation. The characteristic size of the craze microstructure is quite small, on the order of 10^1 nm. On this scale, a contribution from surface tension can give rise to stresses comparable to the polymer yield stress. In terms of hydrodynamic interactions between neighboring fingers, we separate two limiting cases of strongly interacting and noninteracting fingers. In the latter case, each finger propagates independently.

At this point, it might be useful to compare the assumptions of the present model with the earlier model of Kramer et al.[24,25] Similar to Kramer's model, our model treats the craze-thickening process as a process of growth of void fingers inside a polymeric material, which is described as a viscous fluid. We also make a similar assumption that hydrodynamic interactions and surface tension determine finger propagation. However, as we will see later, the models differ substantially in the formulation of the finger propagation problem. The other crucial difference is related to the interpretation of surface tension, which is a scale-dependent function in our model. As the result of these differences, the model predictions in many cases differ substantially from the work of Kramer et al. A detailed description of these results is given in sections 7 and 8.

In the present work, we are interested in determining the dependence of various craze microstructural parameters such as finger radius r, distance between fingers D_0, draw ratio λ_m, and craze-thickening stress σ_0 on imposed strain rate, temperature, and various material properties. We also want to determine the influence of the geometrical size of the sample on the craze propagation and, in particular, the value of the minimal thickness of the film or fiber that still can support steady-state 3D craze propagation.

3. Surface Tension

As was stated above, surface tension plays an important role in defining craze structure on small scales. However, the precise definition of the surface tension on such scales may require some clarification. Indeed, the characteristic diameter of the void fingers considered in the model is on the order of 10^1 nm and thus comparable to the distance between entanglements in a polymer network.[28,33] Since surface tension has a physical meaning of the energy necessary to create a unit area of the new surface inside the material, it must

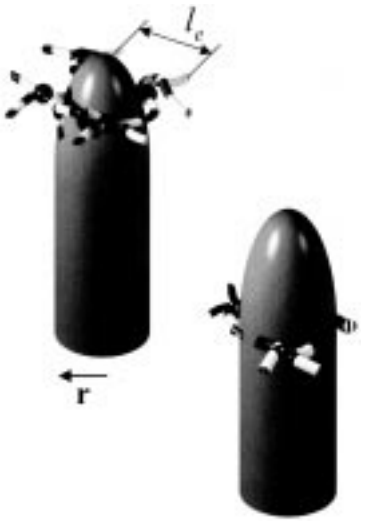

Figure 5. Finger propagating through the entangled polymer network with the distance between entanglements l_e. The chains that happened to be in its way become elongated. If the finger is thick enough, some of these chains have to be broken.

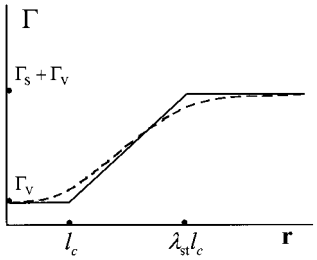

Figure 6. Schematic representation of the dependence of the surface tension Γ on the finger radius r. A dashed curve schematically represents the actual $\Gamma(r)$, while a solid curve corresponds to its approximation defined by eq 1.

be defined in conjunction with the particular process of surface creation. In our case, finger propagation plays the role of such a process. As the finger propagates through the entangled polymer network with the distance between entanglements l_e, the chains that happen to be in its way become elongated, as schematically shown in Figure 5. Although in Figure 5 the polymer network is shown in a grossly oversimplified manner, with the entanglements represented as pointlike objects, the general idea appears quite clear: the energy necessary to propagate the finger must depend on its radius. Indeed, if the radius r of the finger is very large, that is, $r \gg \lambda_{st} l_e$, where λ_{st} is the maximum microscopically allowed entanglement strand elongation ratio, then the entanglement strands that lie in the path of the propagating finger must be broken. On the other hand, if $r \ll l_e$, no appreciable chain scission is necessary in order to propagate the finger. Thus, we can think of surface tension Γ as a scale-dependent quantity $\Gamma(r)$. For the case of large $r \gg \lambda_{st} l_e$, the surface tension Γ has two contributions; one, Γ_s, is due to chain scission, and the other, Γ_V, is due to regular intermolecular (e.g., Van der Waals) interactions. For the case of small $r \ll l_e$, the surface tension Γ only has contributions from Γ_V, as shown schematically in Figure 6. The characteristic length l_c at which the transition between these two values occur must be on the order of l_e, since this is the length scale at which appreciable chain stretching during finger propagation becomes necessary. In the subsequent discussion, we will approximate $\Gamma(r)$ by the following piecewise linear function that satisfies a known asymptotic behavior of $\Gamma(r)$ at large and small r

$$\Gamma(r) = \begin{cases} \gamma_0 + \gamma_1 & \text{if } r/l_c < 1 \\ \gamma_0 + \gamma_1 r/l_c & \text{if } 1 \le r/l_c \le \lambda_{st} \\ \gamma_0 + \gamma_1 l_{st} & \text{if } r/l_c > \lambda_{st} \end{cases} \quad (1)$$

where

$$\gamma_1 = \Gamma_V \left(1 + \frac{\gamma_0}{\gamma_1}\right)^{-1} \quad (2)$$

$$\frac{\gamma_0}{\gamma_1} = -\frac{\Gamma_V}{\Gamma_s}\left(1 - \lambda_{st} + \frac{\Gamma_s}{\Gamma_V}\right) \quad (3)$$

and l_c is taken to be equal to l_e; see Figure 6. Let us now estimate an order of magnitude for Γ_s. As we will see in section 6, all that we actually need to know is whether Γ_s is larger than $(\lambda_{st} - 1)\Gamma_V$. In case where $\Gamma_s > (\lambda_{st} - 1)\Gamma_V$, only Γ_V will enter the final equations. The value of Γ_s can be estimated as $\Gamma_s = W_f/S_f$, where W_f is the energy necessary to break the chains while propagating the finger by some distance L, and S_f is the new surface area created during this process. The number of broken strands can be estimated as $2rLl_e\nu/2$, where r is finger radius, l_e is entanglement distance, and ν is entanglement density. Thus Γ_s can be expressed as

$$\Gamma_s = \frac{W_f}{S_f} \approx \frac{W_0\,(2rLl_e\nu/2)}{2\pi rL} = \frac{l_e \nu W_0}{2\pi} \quad (4)$$

where W_0 is the energy necessary to break one chain strand between entanglements. The value of W_0 can be estimated as $W_0 = UN^*$, where U is the polymer backbone bond energy and N^* is the effective number of monomers along the chain at which the breaking stress is delocalized. In principle, the value of N^* can be anywhere between 1 (stress localized at one bond) and N_e, the number of monomers between entanglements. One can find two different assumptions about the value of N^* in the literature. In the work[25] on crazing in polymers, Kramer assumes that $N^* = 1$, that is, that the stress is localized at one bond. This leads to a rather low value of $\Gamma_s \approx 10^{-2}$ J m^{-2}. On the other hand, in the work of Raphaël and de Gennes[41] on cross-linked polymers, stress is assumed to be delocalized along the whole piece of the chain between cross-links. The actual value of N^* relevant to our problem can be obtained from the experimental data. Thus, from the work[29] on chain scission at diblock reinforced interfaces between PS and PVP, one can obtain $W_0 = (2 \pm 1) \times 10^{-16}$ J. Taking $U = 6 \times 10^{-19}$ J from Kramer and Berger,[24] we obtain $N^* = 330 \pm 160$, which is quite close to PS/PVP diblock $N_e = N_e^{(PS)} + N_e^{(PVP)} = 420$. If we assume that this result reflects the general situation of $N^* \approx N_e$, we can use eq 4 to estimate the value of Γ_s for any polymer provided we know its ν, l_e, and N_e. For PS, we can estimate Γ_s as 5 J m^{-2}, which is much larger than the characteristic value of $\Gamma_V \approx 0.04$ J m^{-2} reported previously.[24] Thus, in the rest of the paper, we will assume that condition $\Gamma_s > (\lambda_{st} - 1)\Gamma_V$ is satisfied.

4. Noninteracting Fingers

Let us first consider the case where the hydrodynamic interactions between propagating fingers is so small that we can neglect it, as it would be in the case of

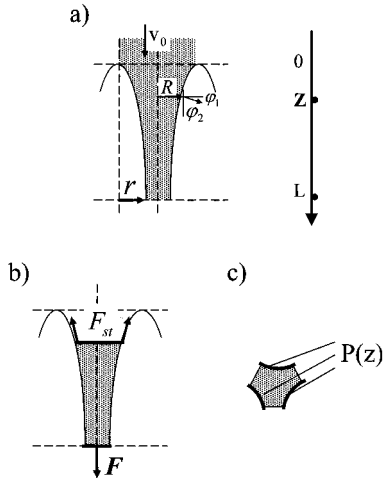

Figure 7. (a) Void fingers tightly packed in space. We can treat their propagation as the process of fiber drawing. (b) Fiber between planes $z = z$ and $z = L$ subject to surface tension force F_{st} and applied force F. (c) Length of the boundary $P(z)$ along which surface tension force F_{st} is acting on the fiber cross section at point z.

considerable spatial separation of the fingers. In this case, each finger propagates independently of its neighbors. We want to calculate the relationship between the applied stress and the finger propagation velocity. We assume that the top of the finger has an ellipsoidal shape and that the finger propagates with constant velocity v_0; see Figure 4. Since we describe our polymer as a Newtonian fluid with viscosity η, the pressure at point A at the top of the finger is equal to[38]

$$p_A^{(1)} = p_0 + a_2 \eta v_0 / r \tag{5}$$

where $p_0 < 0$ is the applied pressure, v_0 is the finger propagation velocity, r is the finger radius, and $a_2 \approx 1$ is a dimensionless parameter that generally depends on the particular shape of the finger cap. However, the dependence of a_2 on the shape is rather weak,[38,39] and for our purposes, we can approximate a_2 as that of a gas bubble, i.e., $a_2 = 1$. In the case of steady-state propagation, the pressure $p_A^{(1)}$ has to be equal to the pressure due to the surface tension

$$p_A^{(2)} = -a_1 \Gamma(r)/r_t \tag{6}$$

where r_t is the local radius of curvature of the surface at point A, $\Gamma(r)$ is surface tension, and a_1 is a dimensionless parameter that for the case of an ellipsoidal cap is equal to 2. Also, for the ellipsoid we have

$$r_t = r^2/L \tag{7}$$

Thus, combining eqs 5−7, we obtain the following relationship between the velocity and the applied stress

$$\frac{v_0}{u'} = \frac{\rho'}{\alpha}\frac{r}{l_c} - \frac{a_1}{2}\frac{\Gamma(r)}{\gamma_1} \tag{8}$$

where

$$u' = 2\gamma_1 \alpha / a_2 \eta \quad \rho' = \sigma_0 l_c / 2\gamma_1 \quad \sigma_0 = -p_0 \quad \alpha = L/r$$

As we can see in the case of noninteracting fingers, the velocity v_0 is a linear function of the applied stress σ_0. Of course, we should bear in mind that the linearity of $v_0(\sigma_0)$ dependence is a consequence of the linear viscous fluid approximation. In case of a nonlinear viscous fluid, the dependence of v_0 on σ_0 takes a more complicated form.

5. Strongly Interacting Fingers

Our next step is to consider the case where the fingers are interacting very strongly, as they might be if they are tightly packed in space. Then, we can look at the finger propagation from another point of view and treat it essentially as the process of drawing of a fiber from the material between void fingers as shown in Figure 7a. As in the case of noninteracting fingers, we describe the polymer as a Newtonian fluid and thus have

$$\sigma_{ii} = -p + 2\eta \frac{\partial v_i}{\partial i} \tag{9}$$

where σ_{ii} is the diagonal part of the stress tensor, p is pressure, η is viscosity, v is fluid velocity, and i corresponds to radial R or longitudinal z coordinate. We assume an elongational flow

$$\frac{\partial v_R}{\partial R} = -{}^1/_2 \frac{\partial v_z}{\partial z} \tag{10}$$

We also assume that the material flux Q is conserved along the fiber and neglect variation of the stress and velocity along the fiber cross section. We then have

$$v_0 S_0 = v_z(z) S(z) = Q = \text{const} \tag{11}$$

where S_0 is the cross-sectional area at the beginning of the fiber, $S(z)$ is the cross-sectional area at point z along the fiber, and v_0 is the finger propagation velocity. We define the draw ratio λ at point z along the fiber as

$$\lambda(z) = S_0/S(z) \tag{12}$$

We can now write a force balance equation for the piece of the fiber between planes $z = L$ and $z = z$; see Figure 7b. We have

$$F = -(F_{st})_z + \sigma_{zz}(z) S(z) \tag{13}$$

where F is the total force applied, $\sigma_{zz}(z)$ is the normal stress component at point z, $S(z)$ is the cross-sectional area at point z, and F_{st} is the surface tension force. Projection of the surface tension force vector is equal to

$$(F_{st})_z = -\Gamma P(z) \cos(\varphi_1) \tag{14}$$

where Γ is surface tension, φ_1 is the angle between F_{st} and the z axis, and $P(z)$ is the length of the boundary along which the surface tension is acting; see Figure 7c. We thus have

$$S(z)\sigma_{zz}(z) = F - \Gamma P(z) \cos(\varphi_1) \tag{15}$$

We now assume Laplace−Young boundary condition

$$f_n = \frac{\beta \Gamma}{r_1(z)} \tag{16}$$

where f_n is the normal component of the force acting on the surface of the fluid, $r_1(z)$ is the radius of the mean surface curvature at point z, Γ is surface tension, and β

is a dimensionless constant on the order of 1 that depends on the particular shape of the surface. This boundary condition can be expressed as

$$\sigma_{zz}\cos^2(\varphi_2) + \sigma_{RR}\cos^2(\varphi_1) = \beta\Gamma/r_1 \qquad (17)$$

where φ_1 and φ_2 are angles between the vector $\vec{n}$ normal to the surface and the z and R axes, respectively; see Figure 7a. Combining eq 15 and 17, we obtain

$$3\eta\cos^2(\varphi_1)\frac{\partial v_z}{\partial z} - \frac{v_z}{v_0}\left(\sigma_0 - \frac{\Gamma P(z)}{S_0}\cos(\varphi_1)\right) + \frac{\beta\Gamma}{r_1} = 0 \qquad (18)$$

where $\sigma_0 = \sigma(z = 0) = F/S_0$. This equation is too complicated to be solved analytically, so we now consider a special case of considerably elongated fingers where $\alpha = L/r \gg 1$. In this case, we can make the following approximations

$$\cos(\varphi_1) \approx 1 \quad r_1(z) \approx r_1(z = L) = r$$
$$P(z) \approx P(z = L) = \pi r \quad \beta \approx 1 \qquad (19)$$

These approximations are good everywhere except for the very top of the finger, where our initial assumption that v and σ are functions of z only breaks down anyway. We thus have

$$3\eta\frac{\partial v_z}{\partial z} - \frac{v_z}{v_0}\left(\sigma_0 - \frac{\pi r\Gamma}{S_0}\right) + \frac{\beta\Gamma}{r} = 0 \qquad (20)$$

This equation can be rewritten in dimensionless form as

$$\frac{\partial(v_z/u)}{\partial(z/L)} - \rho\frac{(v_z/u)}{(v_0/u)} + 1 = 0 \qquad (21)$$

where

$$u = \frac{\alpha\beta\Gamma}{3\eta} \quad \rho = \frac{\sigma_0 L}{\alpha\beta\Gamma} - \frac{\pi r^2}{\beta S_0} \quad \alpha = \frac{L}{r}$$

The solution takes the form

$$v_z = \frac{v_0}{\rho} + v_0\left(1 - \frac{1}{\rho}\right)\exp\left(\frac{\rho u z}{v_0 L}\right) \qquad (22)$$

We also have

$$v_z(z = L) = \lambda_m v_0 \qquad (23)$$

where $\lambda_m = \lambda(z = L)$. Substituting eq 23 into eq 22, we obtain

$$\frac{v_0}{u} = \rho\ln^{-1}\left(\frac{\lambda_m\rho - 1}{\rho - 1}\right) \qquad (24)$$

Let us now expand eq 24 around $1/\rho = 0$. Retaining only the first two terms in the expansion we obtain

$$\frac{v_0}{u} = \frac{\rho}{\ln\lambda_m} - \frac{1 - \lambda_m^{-1}}{\ln^2\lambda_m} \qquad (25)$$

It is easy to demonstrate that for the range of λ_m encountered in experiment (i.e., $2 \lesssim \lambda_m \lesssim 5$) eq 25 reasonably well approximates eq 24 not only at $\rho \gg 1$ but essentially at all ρ, except those where $(\rho - 1) \ll 1$. In our further calculations, we will use eq 25 with the additional condition $\rho - 1 \gtrsim 1$. We can rewrite eq 25 in the same variables as eq 8 for noninteracting fingers

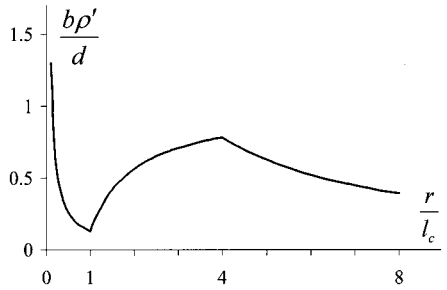

Figure 8. Plot of function $\rho'(r)$ defined by eq 30. The values of material parameters chosen correspond to PS, i.e., $\Gamma_V = 0.04$ J m^{-2}, $\Gamma_s = 5$ J m^{-2}, $\lambda_m = 4$, $\alpha = 6$, and $v_0\eta = 0.5$ J m^{-2}. See section 8 for details.

$$\frac{v_0}{u'} = \frac{a_2\rho' r}{3l_c\ln\lambda_m} - \frac{\beta a_2\Gamma(\lambda_m - 1)}{6\gamma_1\lambda_m\ln\lambda_m}\left(\frac{2}{\beta} + \frac{1}{\ln\lambda_m}\right) \qquad (26)$$

where

$$u' = \frac{2\gamma_1\alpha}{a_2\eta} \quad \rho' = \frac{\sigma_0 l_c}{2\gamma_1} \quad \alpha = \frac{L}{r} \gg 1$$
$$\rho = \frac{2r\gamma_1\rho'}{\beta l_c\Gamma} - \frac{2}{\beta}\left(1 - \frac{1}{\lambda_m}\right) \gtrsim 2 \qquad (27)$$

We see from eq 26 that, similar to the case of noninteracting fingers, the propagation velocity of strongly interacting fingers is a linear function of the applied stress.

6. Fastest Propagating Fingers

In the previous two sections, we estimated the finger propagation velocity in the limits of tightly packed (strongly interacting) and spatially separated (noninteracting) fingers. The finger separation D_0 can easily be expressed in terms of the finger radius r and the draw ratio λ_m as (see Appendix)

$$\left(\frac{D_0}{r}\right)^2 = \frac{2\pi}{\sqrt{3}}\frac{\lambda_m}{\lambda_m - 1} \qquad (28)$$

As we see, the case $\lambda_m - 1 \ll 1$ corresponds to strongly separated fingers, and $\lambda_m - 1 \gg 1$ to tightly packed fingers. Thus, we can summarize eqs 8 and 26 as

$$\frac{v_0}{u'} = \begin{cases} b\rho' r/(2l_c) - d\Gamma(r)/(2\gamma_1) & \text{if } \lambda_m - 1 \gg 1 \\ \rho' r/(\alpha l_c) - a_1\Gamma(r)/(2\gamma_1) & \text{if } \lambda_m - 1 \ll 1 \end{cases} \qquad (29)$$

where

$$b = \frac{2a_2}{3\ln\lambda_m} \quad d = \frac{\beta a_2(\lambda_m - 1)}{3\lambda_m\ln\lambda_m}\left(\frac{2}{\beta} + \frac{1}{\ln\lambda_m}\right)$$
$$u' = \frac{2\gamma_1\alpha}{a_2\eta} \quad \rho' = \frac{\sigma_0 l_c}{2\gamma_1}$$

$a_1 = 2$, $a_2 = 1$, $\beta = 1$, and $\Gamma(r)$ is defined by eq 1. Our next goal is to determine parameters r and λ_m that correspond to the fastest propagating fingers or, equally speaking, to the fingers that require the lowest stress to propagate.

Let us first consider the case of tightly packed fingers, where $\lambda_m - 1 \gg 1$. Substituting eq 1 into eq 29, we obtain

$$\frac{b\rho'}{d} = \begin{cases} [\gamma_0/\gamma_1 + 2v_0/(du') + 1]l_c/r & \text{if } r/l_c < 1 \\ [\gamma_0/\gamma_1 + 2v_0/(du')]\ l_c/r + 1 & \text{if } 1 \le r/l_c \le \lambda_{st} \\ [\gamma_0/\gamma_1 + 2v_0/(au') + \lambda_{st}]\ l_c/r & \text{if } r/l_c > \lambda_{st} \end{cases} \quad (30)$$

From eq 3, we know that if $\Gamma_s > (\lambda_{st} - 1)\Gamma_V$ we have

$$-1 < \gamma_0/\gamma_1 < 0 \quad (31)$$

We assume that the velocity v_0 is low enough to satisfy

$$\gamma_0/\gamma_1 + 2v_0/(du') < 0 \quad (32)$$

Then function ρ' defined by eq 30 has a minimum at $r = l_c$, as shown in Figure 8. A similar situation happens in case of noninteracting fingers, where $\lambda_m - 1 \ll 1$. Substituting eq 1 into eq 29, we obtain

$$\frac{2\rho'}{\alpha a_1} = \begin{cases} [\gamma_0/\gamma_1 + 2v_0/(a_1u') + 1]l_c/r & \text{if } r/l_c < 1 \\ [\gamma_0/\gamma_1 + 2v_0/(a_1u')]l_c/r + 1 & \text{if } 1 \le r/l_c \le \lambda_{st} \\ [\gamma_0/\gamma_1 + 2v_0/(a_1u') + \lambda_{st}]l_c/r & \text{if } r/l_c > \lambda_{st} \end{cases} \quad (33)$$

In the case where

$$\gamma_0/\gamma_1 + 2v_0/(a_1u') < 0 \quad (34)$$

the function ρ' defined by eq 33 has a minimum at $r = l_c$. Thus, we can see that at low velocities the lowest stress ρ' is required for propagation of fingers with radius $r = l_c$. We can now rewrite eq 29 as the following

$$\rho' = \begin{cases} [2v_0/u' + d(\gamma_0/\gamma_1 + 1)]/b & \text{if } \lambda_m - 1 \gg 1 \\ \alpha[2v_0/u' + a_1(\gamma_0/\gamma_1 + 1)]/2 & \text{if } \lambda_m - 1 \ll 1 \end{cases} \quad (35)$$

Analysis of this equation shows that it depends on Γ_V but not on Γ_s. This is due to the fact that the fingers with $r = l_c$ experience only Van der Waals surface tension Γ_V, and thus Γ_s does not enter the equation for the finger propagation stress. In our model, we consider the case of steady-state propagation. In this case, the finger propagation velocity v_0 is defined by the draw ratio λ_m and by the fiber take-up velocity (sample elongation velocity) v_{ext}, which is determined by the experimental setup. The dependence takes the form[1]

$$v_0 = v_{ext}/(\lambda_m - 1) \quad (36)$$

Then, function ρ' described by eqs 35 and 36 is a decreasing function of λ_m, as shown in Figure 9. Thus, the higher the value of λ_m, the lower the stress ρ' required to propagate the fingers. The maximum value that λ_m can attain is λ_{st}, the maximum microscopically allowed entanglement strand extension.[1,24,25] Thus the lowest stress of finger propagation is obtained at $\lambda_m = \lambda_{st}$.

The results we have obtained for the fastest propagating fingers can be summarized as

$$r = l_c \quad (37)$$

$$\lambda_m = \lambda_{st} \quad (38)$$

$$\rho' = \begin{cases} [2v_0/u' + d(\gamma_0/\gamma_1 + 1)]/b & \text{if } \lambda_m - 1 \gg 1 \\ [2v_0/u' + a_1(\gamma_0/\gamma_1 + 1)]\alpha/2 & \text{if } \lambda_m - 1 \ll 1 \end{cases} \quad (39)$$

where the following is assumed

$$v_0/u' < -\gamma_0 a_1/(2\gamma_1) \quad \text{if } \lambda_m - 1 \ll 1 \quad (40)$$

$$v_0/u' < -\gamma_0 d/(2\gamma_1) \quad \text{if } \lambda_m - 1 \gg 1 \quad (41)$$

$$\rho = 2\gamma_1\rho'/[\beta(\gamma_0 + \gamma_1)] - 2(\lambda_m - 1)/(\beta\lambda_m) \gtrsim 2 \quad \text{if } \lambda_m - 1 \gg 1 \quad (42)$$

$$0 < -\gamma_0/\gamma_1 < 1 \quad \alpha = L/r \gg 1$$

with b, d, u', ρ', a_1, a_2, and β as defined beneath eq 29. Thus, we have estimated the finger radius, draw ratio, and drawing stress for the fastest propagating fingers. Assuming that these fingers ultimately determine the observed craze structure, we can attempt to compare our results with the experimental data. This comparison constitutes the topic of the next two sections.

7. Craze Microstructure

Let us now compare the predicted craze microstructural parameters, i.e., draw ratio λ_m and finger radius r, with the experimental data. The prediction of the model that $\lambda_m = \lambda_{st}$ is the same as in the earlier models of crazing[24,25] and is clearly supported by experimental data,[24] which generally give $\lambda_m \approx 0.9\lambda_{st}$. However, the prediction that $r = l_c = l_e$, where l_e is the distance between entanglements, is new with respect to earlier models. Thus, it warrants a check against available experimental data. Craze microstructural parameters, such as craze fibril diameter d_1 and draw ratio λ_m, were measured by Berger[32] for a number of glassy polymers. In our model, the fibril diameter d_1 is uniquely defined by the finger radius r and draw ratio λ_m (see Appendix)

$$d_1 = 2D_0\left\{\frac{1}{3} + \frac{\sqrt{3}}{2\pi}\left(1 - \frac{1}{\lambda_m}\right) - \left[\frac{\sqrt{3}}{2\pi}\left(1 - \frac{1}{\lambda_m}\right)\right]^{1/2}\right\}^{1/2}$$

$$D_0 = r\left[\frac{\sqrt{3}}{2\pi}\left(1 - \frac{1}{\lambda_m}\right)\right]^{-1/2} \quad (43)$$

Substituting data for λ_m and $r = l_e$ from Berger,[32] we obtain the results shown in Table 1. As we can see, the agreement is reasonable for the majority of polymers, except for pure PS and the PPO−PS blends with the low molecular weight $M_w = 4K$. The discrepancy for PPO−PS ($M_w = 4K$) is not surprising, since at such low molecular weights chain disentanglement and pullout might play a significant role. The origin of the 25% difference between the value of d_1 for PS calculated from eq 43 and its experimental value is not immediately

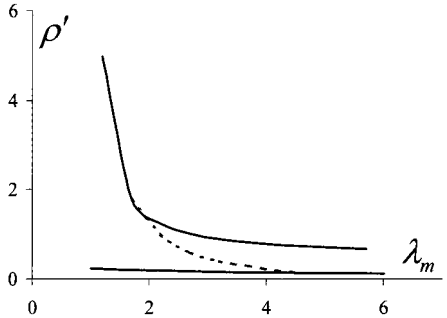

Figure 9. Plot of function $\rho'(\lambda_m)$ defined by eq 35. Solid lines correspond to two different limits of eq 35, and the dashed line schematically indicates a transition between them. The values of parameters are chosen to be the same as those in Figure 8.

Table 1. Distance between Entanglements l_e, Fibril Draw Ratio λ_m, and Fibril Diameter d_1 for Various Polymers[a]

material	l_e [nm]	λ_m	$d_1^{(exp)}$ [nm]	$d_1^{(th)}$ [nm]
PαMS	8.6	3.5	11.5	11.4
PMMA	7.3	2.0	12.5	12.4
PS	9.6	4.0	9.5	12.3
PPO−PS (M_w = 90K)				
ϕ(PPO) = 0.2	8.0	3.6	10.0	10.5
ϕ(PPO) = 0.4	7.2	3.3	10.3	9.7
PPO−PS (M_w = 4K)				
ϕ(PPO) = 0.6	8.0	3.5	13.1	10.6
ϕ(PPO) = 0.7	7.0	3.3	14.7	9.4

[a] Theoretical values of d_1 are calculated using eq 43. Experimental values of d_1 are from refs 32 and 33.

clear. Generally, crazing stress and craze microstructural parameters for pure PS measured by different authors[24,28,29] show considerable variations, which makes it reasonable to assume that details of the sample preparation technique can substantially influence the crazing properties of pure PS.

8. Crazing Stress

We now want to compare eq 39 for the craze-thickening stress σ_0 with the experimental data. We first rewrite eq 39 in the original notations

$$\sigma_0 = \begin{cases} [a_2 v_0 \eta/(\alpha l_c) + d\Gamma_V/l_c]2/b & \text{if } \lambda_m - 1 \gg 1 \\ [a_2 v_0 \eta/(\alpha l_c) + a_1 \Gamma_V/l_c]\alpha & \text{if } \lambda_m - 1 \ll 1 \end{cases} \quad (44)$$

where b, d, α, a_2, a_1, and β as defined previously. In our model, we have only one adjustable parameter α, and it describes the elongation of the ellipsoidal finger cap. Let us now estimate the value of α. Substituting data[1,24] for PS as $\Gamma_V = 4 \times 10^{-2}$ N m^{-1}, $\lambda_m = 4$, $l_c = 9.6$ nm, $v_0\eta = 0.5$ N m^{-1}, and $\sigma_0 = 40$ MPa in eq 44, we obtain $\alpha = 6$. For eq 44 to be valid, eqs 40−42 must be satisfied. We can rewrite these restrictions as the following

$$\eta v_0 < -\gamma_0 \alpha a_1/a_2 \quad \text{if } \lambda_m - 1 \ll 1$$

$$\eta v_0 < -\gamma_0 \alpha d/a_2 \quad \text{if } \lambda_m - 1 \gg 1$$

$$\sigma_0 l_c \gtrsim 2\Gamma_V(\beta + 1 - 1/\lambda_m) \quad \text{if } \lambda_m - 1 \gg 1 \quad (45)$$

Substituting the same values of material parameters as above in eq 45 and using eqs 1−3 for γ_0, we easily verify that the conditions in eq 45 are satisfied.

Let us now calculate σ_0 as a function of the density of entanglements ν. To do this, we use the following phenomenological relationships[24,25]

$$l_c = l_e \approx c_1 \nu^{-1/2} \quad (46)$$

$$\lambda_m \approx c_2 \nu^{-1/2} \quad (47)$$

where $c_1 \approx 5.2 \times 10^4$ m$^{-1/2}$ and $c_2 \approx 2.4 \times 10^{13}$ m$^{-3/2}$. Substituting eqs 36, 46, and 47 into eq 44 and using the same values of α and $v_{ext}\eta$ as above, we obtain σ_0 as a function of ν. The plot of this function and appropriate experimental data from refs 24−31 are shown in Figure 10. As one can see for $\nu \lesssim 10 \times 10^{25}$ m^{-3}, the agreement is good, given the substantial scattering of experimental data. The results shown in Figure 10 are obtained using $\alpha = 6$, which was calculated above on the basis of experimental data for PS. It might be interesting to see how robust the model is with respect to variations of

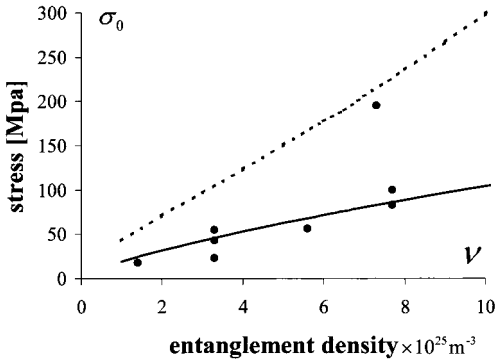

Figure 10. Craze-thickening stress σ_0 as a function of entanglement density ν. Dashed curve corresponds to $\lambda_m - 1 \ll 1$ limit of eq 44, and solid curve corresponds to $\lambda_m - 1 \gg 1$ limit. Experimental points are from refs 24−31.

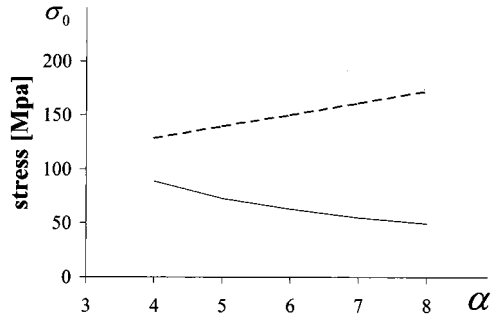

Figure 11. Craze-thickening stress σ_0 as a function of adjustable parameter α for entanglement density $\nu = 5 \times 10^{25}$ m^{-3}. Dashed curve corresponds to $\lambda_m - 1 \ll 1$ limit of eq 44, and solid curve corresponds to $\lambda_m - 1 \gg 1$ limit.

the value of α. In Figure 11, function $\sigma_0(\alpha)$ is shown for $\nu = 5 \times 10^{25}$ m^{-3}. As one can see from this figure, σ_0 is not particularly sensitive to changes in α, indicating that the model predictions are not substantially affected by the particular value of α chosen.

For $\nu \gtrsim 10 \times 10^{25}$ m^{-3}, the model predictions do not agree with the experimental data. The most obvious explanation of this discrepancy is that under regular testing conditions ($T \approx 23$ °C, $v_{ext} \approx 10^{-6}$−10^{-4} m/s) polymers with $\nu > 10 \times 10^{25}$ m^{-3} cannot develop pure crazes, and thus experimental measurements are performed on samples with the mixed-mode deformation, i.e., those containing both plastic deformation zones and craze regions. Interpretation of such measurements requires considerable caution and probably cannot be performed directly in terms of the present model. The other contribution to the above-mentioned discrepancy comes from the fact that eqs 46 and 47 have to be modified for high values of ν, since they are based on the Gaussian chain approximation. At high ν, however, the chain strands between entanglements are too short to be Gaussian and must be described by Porod−Kratky or similar inextensible models. Additional complications can arise if a special treatment such as cold drawing or physical aging is used to promote crazing in high-entanglement-density materials. Such treatments can dramatically change polymer network structure and behavior above the yield point. To be applicable in these situations, the model might require substantial modifications that would take into account changes introduced to these materials. Finally, we should bear in mind that as we move to the polymers with higher and higher entanglement densities, experimental data[42] indicate that for such materials relative contributions

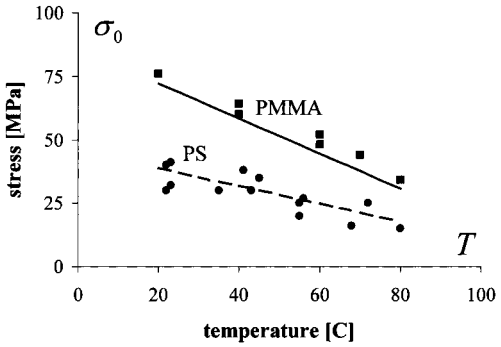

Figure 12. Craze-thickening stress σ_0 as a function of temperature T for PS and PMMA. Solid line corresponds to eq 44. Experimental points are from refs 24,26.

of strain and strain rate terms to the constitutive stress-strain relationship (see eq 1 of Part 1) becomes on the same order of magnitude. This indicates that at some point our assumption that the material can be treated simply as a viscous fluid breaks down, and the model must be modified to include both terms in eq 1 of Part 1.

Equation 44 can also be used to estimate the dependence of σ_0 on temperature T. To do this, we must first obtain the dependence of the effective viscosity η on T, since η is the only quantity in eq 44 that can appreciably depend on T for temperatures considerably lower than the glass-transition temperature T_g. Since most experiments are performed on a relatively narrow temperature interval,[26,27] the simplest approach is to use Taylor expansion of the function $\eta(T)$ around some characteristic temperature below T_g. Retaining only two first terms in Taylor expansion, we obtain a linear dependence of η on T that can be expressed in the form

$$\eta(T) = k_1 + k_2(T_g - T) \tag{48}$$

where k_1 and k_2 are some constants. A similar assumption was also used in some earlier works on crazing.[24] We can use eqs 44 and 48 to determine k_1 and k_2 from the known values of $\sigma_0(T)$ for PS; see Figure 12. If we now assume that the values of k_1 and k_2 do not change dramatically from one material to another, we can attempt to estimate $\sigma_0(T)$ for some other polymer, say PMMA, by substituting[26] $\nu_{PMMA} = 7.8 \times 10^{25}$ m^{-3} in eq 44. The results are shown in Figure 12. As we can see, the agreement with experimental results is good.

Equation 44 also allows us to discuss craze-to-shear transition as a function of temperature T and density of entanglements ν. Craze-to-shear transition occurs when crazing stress σ_0 becomes larger than shear initiation stress (yield stress) σ_y. Since σ_y depends linearly on the temperature[24-27] and approaches zero at T_g, it can be approximated as

$$\sigma_y = k_3(T_g - T) \tag{49}$$

Then, from eqs 44, 48, and 49, we can obtain the following equation for transition temperature T_{tr} at which $\sigma_y = \sigma_0$

$$T_g - T_{tr} = \begin{cases} (a_2k_1\nu_0 + \alpha d\Gamma_{VdV})/(\alpha b l_c k_3/2 - a_2k_2\nu_0) & \text{if } \lambda_m - 1 \gg 1 \\ (a_2k_1\nu_0 + \alpha a_1\Gamma_{VdV})/(l_c k_3 - a_2k_2\nu_0) & \text{if } \lambda_m - 1 \ll 1 \end{cases} \tag{50}$$

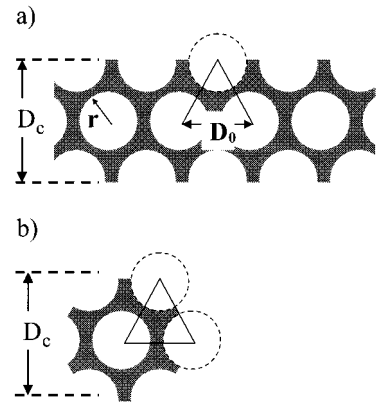

Figure 13. (a) 3D craze in a film must contain at least one raw of fingers. (b) 3D craze in a fiber must contain at least one finger. See details in the text.

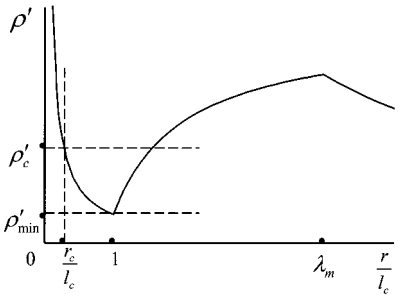

Figure 14. Thin samples where finger radius $r = r_c < l_c$. Finger propagation stress $\rho'(r = r_c)$ is higher than the propagation stress $\rho'(r = l_c)$ that corresponds to fingers in thick samples.

with b, d, α, a_2, a_1, and β as defined previously and λ_m and l_c as defined by eqs 46 and 47. We can now compare eq 50 with the known data[24] on PS. Assuming[24] that $\sigma_y^{PS} = 85$ MPa at 20 °C and using k_1 and k_2 obtained earlier, we can calculate $T_{tr}(\nu)$ for cross-linked PS as shown in Figure 2. As we can see, the agreement with experimental data is good except for T close to T_g, where chain pullout and similar effects become important. Thus, in this section, we calculated crazing stress and craze-to-shear transition stress as a function of entanglement density ν and temperature T. The obtained theoretical predictions are generally in good agreement with the available experimental results.

9. Critical Thickness

The approach developed in section 6 can be used to analyze the phenomenon of critical thickness. Critical thickness refers to the characteristic size of the sample (film or fiber thickness, etc.) below which craze propagation requires stresses higher than the yield stress. We thus need to investigate craze-to-shear transition that occurs as we decrease the sample size. For the regular 3D craze to exist, we need to fit at least one void finger inside the sample, as shown in Figure 13. As was shown in section 6, the lowest stress is required to propagate the finger with the radius $r = l_c = l_e$. Thus for the thin samples that have fingers with $r = r_c < l_c$, craze propagation stress must be higher, as shown in Figure 14. This stress is defined by eqs 30 and 33 with $r = r_c$ and $r/l_c < 1$ as

$$\frac{\sigma_0 l_c}{2\gamma_1} = \begin{cases} [\gamma_0/\gamma_1 + 2v_0/(du') + 1]\, dl_c/(br) & \text{if } \lambda_m - 1 \gg 1 \\ [\gamma_0/\gamma_1 + 2v_0/(a_1 u') + 1]\, \alpha a_1 l_c/(2r) & \text{if } \lambda_m - 1 \ll 1 \end{cases} \quad (51)$$

Critical thickness is achieved when σ_0 defined by eq 51 becomes equal to the deformation zone propagation stress σ_{0y}. Thus, substituting σ_{0y} instead of σ_0 in eq 51 and using eq 43 for D_0, we obtain for critical thickness $D_c \equiv \sqrt{3}D_0$ the following relationship

$$D_c = \begin{cases} [2\pi\sqrt{3}/(1-\lambda_m^{-1})]^{1/2}\,[1 + a_2 v_{ext}\eta/(\alpha d\Gamma_V(\lambda_m - 1))]2d\Gamma_V/(b\sigma_{0y}) & \text{if } \lambda_m - 1 \gg 1 \\ [2\pi\sqrt{3}/(1-\lambda_m^{-1})]^{1/2}\,[1 + a_2 v_{ext}\eta/(\alpha a_1\Gamma_V(\lambda_m - 1))]\alpha a_1\Gamma_V/\sigma_{0y} & \text{if } \lambda_m - 1 \ll 1 \end{cases} \quad (52)$$

In the case where $v_{ext}\eta/(\alpha\Gamma_V) \gg 1$, this equation can be further simplified

$$D_c = \begin{cases} [2\pi\sqrt{3}/(1-\lambda_m^{-1})]^{1/2} 3\ln(\lambda_m) v_{ext}\eta/(\alpha\sigma_{0y}(\lambda_m - 1)) & \text{if } \lambda_m - 1 \gg 1 \\ [2\pi\sqrt{3}/(1-\lambda_m^{-1})]^{1/2} a_2 v_{ext}\eta/(\sigma_{0y}(\lambda_m - 1)) & \text{if } \lambda_m - 1 \ll 1 \end{cases} \quad (53)$$

This equation has the same form as the equation for the maximum thickness of the film that can support stable 2D craze propagation (see eq 33 in Part 1)

$$D_c^{DZ} = 2h_c = \frac{4\eta v_{ext}}{\sigma_{0y}(\lambda_m - 1)} \quad (54)$$

For the range of λ_m encountered in the majority of crazing polymers ($2 \lesssim \lambda_m \lesssim 5$), eqs 54 and 53 differ only by a numerical factor of the order of 1. Let us now compare eqs 54 and 53 with the experimental data on critical thickness in PS−PPO blends.[34−37] Plots of eqs 54 and 53 were calculated using the same values of ηv_{ext} and σ_{0y} as were used before, and the results are shown in Figure 15. As we can see, the agreement is good. One can also see that for $\nu \lesssim 8 \times 10^{25}$ m^{-3} there is a region on the plot (above the eq 53 $\lambda_m - 1 \gg 1$ curve but below the eq 54 curve) where both 2- and 3D crazes can be stable. This region corresponds to the mixed-mode deformation where the system randomly alternates between 3- and 2D modes. This indicates that a transition from 3- to 2D crazing should not be very sharp and should happen over some interval in film thickness. Indeed, experimental data on critical thickness support this prediction.[34−37]

10. Conclusions

In the present work, a simple model of craze thickening in a polymer glass is proposed. The model describes a 3D craze structure as a set of void fingers propagating through the polymer. Craze fibrils are represented by the material pushed between the void fingers. Propagation of these void fingers is assumed to be dominated by the viscous force between fingers and by the scale-dependent surface tension. The model allows successful prediction of the crazing stress and of the details of the 3D craze microstructure. In particular, the average craze fibril diameter d_1 and the natural draw ratio λ_m are expressed as simple functions of the maximum entanglement strand elongation λ_{st} and the average distance between entanglements l_c. Craze-thickening stress σ_0 is calculated as a function of the density of entanglements ν and temperature T. On the basis of this information, a craze-to-shear transition is analyzed. All of these results are in good agreement with experimental data. The theory is also consistent with the observation that 3D crazes can exist only in film thicknesses above some critical thickness. The calculated values of this critical thickness are in good agreement with experimental values and with the values of the critical thickness obtained earlier in the model of 2D crazing described in Part 1 of the present series.

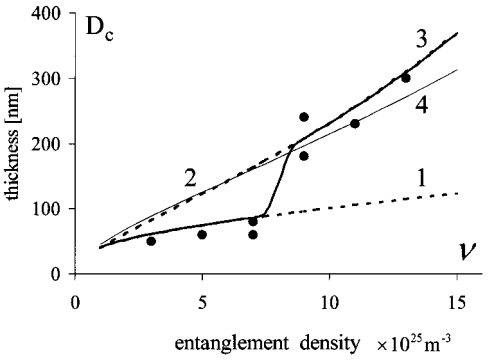

Figure 15. Critical thickness D_c as a function of entanglement density ν. Curves 1 and 2 correspond to two different limits of eq 53. Curve 3 schematically indicates a transition between them. Curve 4 corresponds to eq 54. Experimental points are from refs 34−37.

The fact that 3D craze thickening is suppressed in thin-enough polymer films and fibers potentially bears important practical implications. Indeed, unlike 3D crazes that are very fragile and can easily break giving rise to cracks,[24,25] 2D crazes are quite robust and allow elongation at break close to the maximum microscopically allowed.[14,15,34−37] This phenomenon can be used to develop novel polymeric materials with substantially improved mechanical performance. One interesting possibility is to construct multicomponent polymeric materials that have subcritically thin elements like alternating layers or fibers that do not allow 3D crazing. Such materials can exhibit high toughness and ductility even if their components are quite brittle in the bulk. Analyzes of the mechanical properties of such materials constitute a logical continuation of the present work and will be given in a separate publication.

Acknowledgment. This work was supported by the MRL Program of the National Science Foundation under Award No. DMR96-32716. We thank Profs. Kramer, Donald, and Michler for their helpful comments and discussions.

Appendix

Finger Separation and Fiber Radius. Let us consider three neighboring fingers of radius r shown in Figure 16. The fibril cross section at the top of the neck is a triangle with a side D_0 and area $S_0 = \sqrt{3}D_0^2/4$. The fiber cross section at the bottom of the neck is obtained by subtracting three circular sectors from the triangle, as shown in Figure 16. Thus, the area of the bottom cross section is $S_1 = S_0 - \pi r^2/2$. At the same time, from eq 12, we have $S_0 = \lambda_m S_1$. Combining these equations

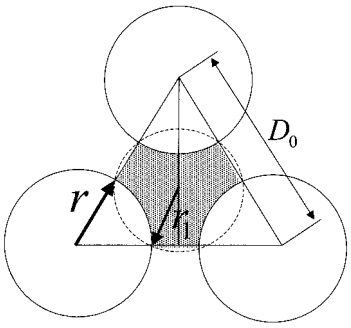

Figure 16. Three neighboring fingers. View from above.

we obtain

$$\left(\frac{D_0}{r}\right)^2 = \frac{2\pi}{\sqrt{3}} \frac{\lambda_m}{\lambda_m - 1} \tag{A1}$$

The radius of the fiber at the bottom of the neck can be defined as the radius r_1 of the smallest circle containing the fiber crossection; see Figure 16. Using simple geometrical arguments, we obtain for r_1 the following equation:

$$r_1 = D_0 \left\{\frac{1}{3} + \frac{\sqrt{3}}{2\pi}\left(1 - \frac{1}{\lambda_m}\right) - \left[\frac{\sqrt{3}}{2\pi}\left(1 - \frac{1}{\lambda_m}\right)\right]^{1/2}\right\}^{1/2} \tag{A2}$$

References and Notes

(1) Krupenkin, T. N.; Fredrickson, G. H. Crazing in Two and Three Dimensions. 1. Two-Dimensional Crazing. *Macromolecules* **1999**, *32*, 5029.
(2) Hui, C. Y.; Kramer, E. J. *Polym. Eng. Sci.* **1995**, *35*, 419.
(3) Yang, C.-M. A.; Kunz, M. S.; Logan, J. A. *Macromolecules* **1993**, *26*, 1767.
(4) Hui, C. Y.; Ruina, A.; Creton, C.; Kramer, E. J. *Macromolecules* **1992**, *25*, 3948.
(5) Brown, H. R. *Macromolecules* **1991**, *24*, 2752.
(6) Miller, P.; Kramer, E. J. *J. Mater. Sci.* **1991**, *26*, 1459.
(7) Brown, H. R.; Njoku, N. G. *J. Polym. Sci., Poly. Phys.* **1986**, *24*, 11.
(8) Michler, G. H. *Colloid Polym. Sci.* **1986**, *264*, 522.
(9) Michler, G. H. *Colloid Polym. Sci.* **1985**, *263*, 462.
(10) Kramer, E. J. *Polym. Eng. Sci.* **1984**, *24*, 761.
(11) Donald, A. M.; Kramer, E. J. *J. Mater. Sci.* **1982**, *17*, 1871.
(12) Wang, W. C. V.; Kramer, E. J. *J. Mater. Sci.* **1982**, *17*, 2013.
(13) Donald, A. M.; Kramer, E. J. *J. Mater. Sci.* **1981**, *16*, 2977.
(14) Donald, A. M.; Chan, T.; Kramer, E. J. *J. Mater. Sci.* **1981**, *16*, 669.
(15) Chan, T.; Donald, A. M.; Kramer, E. J. *J. Mater. Sci.* **1981**, *16*, 676.
(16) Donald, A. M.; Kramer, E. J. *Philos. Mag.* **1981**, *43*, 857.
(17) Lauterwasser, B. D.; Kramer, E. J. *Philos. Mag.* **1979**, *39*, 469.
(18) Argon, A. S.; Salama, M. M. *Philos. Mag.* **1977**, *36*, 1217.
(19) Argon, A. S.; Salama, M. M. *Mater. Sci. Eng.* **1976**, *23*, 219.
(20) Brown, H. R.; Ward, I. M. *Polymer* **1973**, *14*, 469.
(21) Sauer, J. A.; Hara, M. *Adv. Polym. Sci.* **1990**, *91/92*, 70.
(22) Brown, H. R. *Mater. Sci. Rep.* **1987**, *2*, 315.
(23) Fredrich, K. *Adv. Polym. Sci.* **1983**, *52/53*, 225.
(24) Kramer, E. J.; Berger, L. L. *Adv. Polym. Sci.* **1990**, *91/92*, 1.
(25) Kramer, E. J. *Adv. Polym. Sci.* **1983**, *52/53*, 1.
(26) Döll, W.; Könczoll, L. *Adv. Polym. Sci.* **1990**, *91/92*, 137.
(27) Döll, W. *Adv. Polym. Sci.* **1983**, *52/53*, 105.
(28) Donald, A. M.; Kramer, E. J. *J. Polym. Sci., Poly. Phys.* **1982**, *20*, 1129.
(29) Creton, C.; Kramer, E. J.; Hui, C. Y.; Brown, H. R. *Macromolecules* **1992**, *25*, 3075.
(30) Morgan, G. P.; Ward, I. M. *Polymer* **1977**, *18*, 87.
(31) Fraser, R. A. W.; Ward, I. M. *Polymer* **1978**, *19*, 220.
(32) Berger, L. L. *Macromolecules* **1989**, *22*, 3162.
(33) Berger, L. L. *Macromolecules* **1990**, *23*, 2926.
(34) Sanden, Van der; Meijer, H. E. H.; Lamstra, P. J. *Polymer* **1993**, *34*, 2148.
(35) Sanden, Van der; Meijer, H. E. H.; Tervoort, A. *Polymer* **1993**, *34*, 2961.
(36) Sanden, Van der; Meijer, H. E. H. *Polymer* **1993**, *34*, 5063.
(37) Sanden, Van der; Buijs, L. G. C.; Bie, F. O.; Meijer, H. E. H. *Polymer* **1994**, *35*, 2783.
(38) Landau, L. D.; Lifshitz, E. M. *Fluid Mechanics*; Pergamon Press: Oxford, 1987; p 59.
(39) Lamb, H. *Hydrodynamics*; Dover Publications: New York, 1945.
(40) Fields, R. J.; Ashby, M. F. *Philos. Mag.* **1976**, *33*, 33.
(41) Raphaöl, E.; de Gennes, P. G. *J. Phys. Chem.* **1992**, *96*, 4002.
(42) Haward, R. N. *Macromolecules* **1993**, *26*, 5860.

MA9810159